Supplementary Information

A mathematical model to identify optimal combinations of drug targets for dupilumab poor responders in atopic dermatitis

Takuya Miyano, Alan D Irvine and Reiko J Tanaka

1. Selection of clinical studies

We selected clinical studies to be referenced in the QSP model according to pre-defined inclusion and exclusion criteria (FIGURE S1).
We searched the clinical trials that evaluated efficacy of biologic drugs in AD patients, where Ph2 studies were not searched if Ph3 results were available and case reports were not searched if placebo-controlled double-blind clinical trial data were available. We excluded investigational drugs if the clinical efficacies were not evaluated by a placebo-controlled study, if they failed to show a clinical efficacy compared to placebo, if the clinical trials recruited only a small number (<10) of AD patients, if evaluation periods were short (less than 4 weeks), or if data of efficacy endpoints were not published (TABLE S1). When there remained multiple clinical studies per drug, we adopted the clinical study of combination therapy with topical corticosteroids, which is more reflective of the likely clinical use compared with monotherapy, and studies with the largest number of patients.

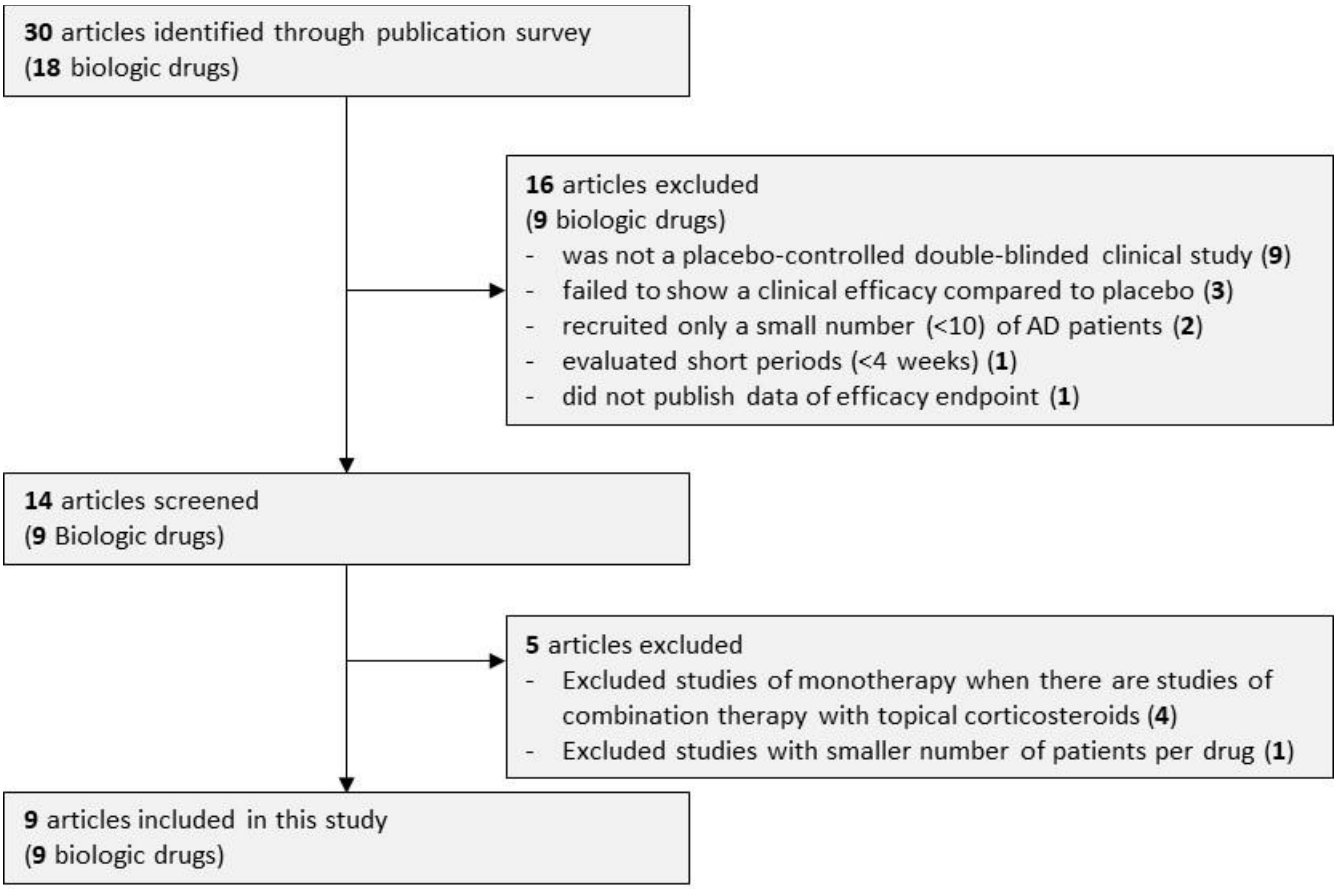

FIGURE S1 Clinical studies selection process

TABLE S1 Drugs excluded in this study

Drugs	Targets	#patients in placebo/drug arm (Phase)	Reasons to be excluded
Omalizumab エラー! 参照元が見つかりません。, 2 (anti-IgE antibody)	IgE	4/4 and 7/13 (Ph4)	• It is difficult to interpret the results due to the small number of patients • Omalizumab showed comparable or lower clinical efficacy than placebo in terms of IGA score and %improved SCORAD (not significant)
Mepolizumab (anti-IL5 antibody)	IL-5	16/18 at baseline 11/11 at week 12 8/6 at week 16 4/4 at week 20 (Ph2)[3] 23/20 (Ph2)[4]	• It is difficult to interpret the results due to the small number of patients after 12 weeks[3] • Evaluation periods were short (2 weeks)[4]
MOR106[5] (anti-IL-17C antibody)	IL-17C	N/A (Ph2)	• Data of the primary endpoint are unavailable • The interim analysis detected a low probability to meet the primary endpoint (%improve EASI)
Etokimab[6] (anti-IL-33 antibody)	IL-33	60/59-61 (Ph2)	Etokimab showed a lower clinical efficacy than placebo in terms of %improve EASI at several dose regimens including the highest dose (not significant)
Tocilizumab[7] (anti-IL-6 antibody)	IL-6	-/3	• Placebo-controlled double-blind clinical trial data are unavailable. • A single-arm trial of three AD patients showed tocilizumab significantly improved the EASI score compared with baseline but it is difficult to interpret the results due to the small number of patients
Ustekinumab (anti-IL-12/23 antibody)	IL-12 and IL-23	27/24-28 (Ph2) [8] 16/16 (Ph2) [9]	Ustekinumab showed only comparable clinical efficacy to placebo in terms of %improve EASI (placebo: 37.5% vs. Ustekinumab: 38.2%-39.8% at week 12, not significant)[8] and SCORAD (less decreased in ustekinumab compared with placebo on average, not significant)[9]
Infliximab (anti-TNFa antibody)	TNFa	-/9[10], 1[11]	Placebo-controlled double-blind clinical trial data are unavailable (A single-arm trial of nine AD patients showed infliximab significantly improved the EASI score compared with baseline)
Etanercept	TNFa	-/2[12], 2[13]	Placebo-controlled double-blind clinical trial data are unavailable
Rituximab (anti-CD20 antibody)	B cells	-/6[14], 2[15], 3[16]	Placebo-controlled double-blind clinical trial data are unavailable (A single-arm trial of six AD patients showed rituximab significantly improved the EASI score compared with baseline)

2. Data processing

2.1. Conversion of reported efficacy endpoints to %improved EASI

All the drugs, except for fezakinumab and rIFNg, reported %improved EASI as an efficacy endpoint.

For fezakinumab, we estimated %improved EASI from %improved SCORAD using a regression curve obtained from the relationship between %improved EASI and %improved SCORAD in clinical trials of multiple drugs[1, 17, 18, 19] (FIGURE S2).

For rIFNg, we substituted %improved EASI by the mean value of the %improved scores of the disease signs evaluated (erythema, induration, excoriations, and lichenification)[20].

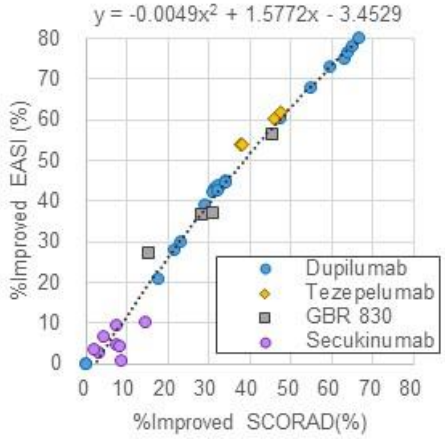

FIGURE S2 Regression curve to estimate %improved EASI from %improved SCORAD

2.2. Normalization of %improved EASI

%improved EASI was normalized to compare clinical efficacies evaluated in different clinical trials. We assumed that the observed %improved EASI is a sum of %improved EASI from net effects of each drug and that from placebo effects, and described normalized %improved EASI, $e_i(t)$, for the *i*-th drug at time *t* by

$$e_i(t) = (e_i^*(t) - e_{\mathrm{P}_i}^*(t)) + e_{\mathrm{P_d}}^*(t). \quad \text{(S1)}$$

The first term corresponds to the difference of the efficacy (%improved EASI) between drug ($e_i^*(t)$) and placebo groups ($e_{\mathrm{P}_i}^*(t)$) to adjust for the different extent of the efficacy in the placebo group in each clinical study due to differences in patient background, concomitant drugs, and sites of study[21]. We then added the same extent of the efficacy in the placebo group ($e_{\mathrm{P_d}}^*(t)$ in the dupilumab clinical trial) in this virtual simulation so that the normalized %improved EASI represents the scale of the observed %improved EASI (the sum of %improved EASI from net effects of each drug and that from placebo effects).

2.3. Normalization of mean EASI score

Normalized mean EASI score was calculated using the baseline mean EASI score (the mean EASI score before the trial) in dupilumab clinical trial[1] and the normalized %improved EASI as follows:

$$a_i(t) = \frac{a_{\mathrm{d}}(0)(100 - e_i(t))}{100} \quad \text{(S2)}$$

where $a_i(t)$ is the normalized mean EASI score of *i*-th drug at *t*, $a_{\mathrm{d}}(0)$ is the reported baseline mean EASI score in the dupilumab clinical trial (the mean value of placebo- and dupilumab-treated groups).

2.4. Normalization of EASI-75 using %improved EASI

Normalized EASI-75 was estimated from the normalized %improved EASI using a regression curve obtained from the relationship between %improved EASI and EASI-75 in clinical trials of multiple drugs[1, 22, 18, 19, 23] (FIGURE S3). The relationship between %improved EASI and EASI-75 is affected by the variation of %improved EASI among the patients. Relatively large deviation of Tezepelumab and GBR 830 in the relationship may derive from the smaller variation between the patients due to the small number of patients in the Ph2 studies compared with the Ph3 studies (dupilumab, nemolizumab, and tralokinumab).

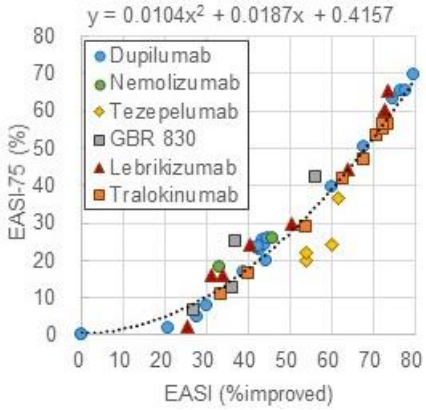

FIGURE S3 Regression curve to estimate EASI-75 from %improved EASI

3. Model structure

The model (FIGURE 2) is formulated by Eqs. (S3)-(S17) shown below. This section details components of the model: EASI score (the output of the model), skin barrier integrity and infiltrated pathogens, cytokines, T cells and drug effects (TABLE S2).

In this model, t is the time after the start of drug treatment. The baseline levels of biological factors (t=0) were obtained from the simulated steady-state level (after 1000 weeks) without any intervention. We referred to the reported levels of biological factors in observational studies as the reference values for the baseline levels, assuming that levels of the biological factors were stable before the start of drug treatments.

TABLE S2 Biological factors as model variables

Factors	Model variables	Reason for inclusion	Reported levels in AD lesion	
			Mean (%CV)	Units
IL-4	$c_4(t)$	Target of dupilumab	38.0 (53) [24 a,d]	Fold change against healthy skin
IL-13	$c_{13}(t)$	Target of dupilumab, tralokinumab, and lebrikizumab	40.5 (56) [24 a,d]	Fold change against healthy skin
IL-17A	$c_{17}(t)$	Target of secukinumab	5.4 (81) [24 a,d]	Fold change against healthy skin
IL-22	$c_{22}(t)$	Target of fezakinumab	3.0 (124)[25 e,d]	Fold change against healthy skin
IL-31	$c_{31}(t)$	Target of nemolizumab	2.0 (49)[25 b,d]	Fold change against healthy skin
IFNg	$c_g(t)$	Target of rIFNg	1.5 (62)[24 a,d]	Fold change against healthy skin
TSLP	$c_{TS}(t)$	Target of tezepelumab	4.4 (76)[26 c]	Fold change against healthy skin
OX40L	$c_{OX}(t)$	Target of GBR 830	9.7 (87)[27 b]	Fold change against AD non-lesion
Th1 cells	$c_{t1}(t)$	Main source of IFNg	3.1 (68)[28, 29 b]	Fold change against AD non-lesion
Th2 cells	$c_{t2}(t)$	Main source of IL-4, IL-13, and IL-31	8.7 (32)[28, 29 b]	Fold change against AD non-lesion
Th17 cells	$c_{t17}(t)$	Main source of IL-17A	2.0 (76)[28, 29 b]	Fold change against AD non-lesion
Th22 cells	$c_{t22}(t)$	Main source of IL-22	21.0 (87)[28, 29 b]	Fold change against AD non-lesion
Infiltrated pathogen	$p(t)$	Key factor in the previous model Its amount is affected by cytokines via AMP	- [e]	-
Skin barrier integrity	$s(t)$	Key factor in the previous model It protects skin from infiltrating pathogens It is related to severity of AD lesion	- [e]	-
EASI score	$e(t)$	Clinical endpoints	29.3 (49)[1 b,d,f]	-

a: mild-to-moderate AD patients. b: moderate-to-severe AD patients. c: both mild-to-moderate and moderate-to-severe AD patients. d: %CV was estimated from IQR. e: no reference data to be compared with simulated values. f: mean baseline value of dupilumab treatment: 29.0 and placebo treatment: 29.6 of AD patients in dupilumab clinical trial

3.1. EASI score, skin barrier integrity, and infiltrated pathogens

We consider EASI as the treatment outcome that will be compared directly to the data from clinical trials.

EASI score (ranging from 0 to 72), is calculated using the severity and the area scores of equally weighted four AD signs (erythema, induration, excoriations, and lichenification) on four body regions (head/neck, trunk, upper limbs, and lower limbs) [30]. In our model, EASI score, $e(t)$, is described (FIGURE S4) by

$$e(t) = 72\,\frac{2p(t)+2(1-s(t))}{4}, \qquad \text{(S3)}$$

where 72 is the maximal EASI score, $p(t)$ is the concentration of infiltrated pathogens with a range from 0 (pathogen-free) to 1 (maximal infiltration) at t, and $s(t)$ is the level of skin barrier integrity with a range from 0 (complete destruction) to 1 (healthy state) at t. Extents of two AD signs (erythema and induration) and those of remaining two signs (excoriations and lichenification) were surrogated by $p(t)$ and 1- $s(t)$, respectively, as described below. We set $e(0) = 29.3$, the baseline EASI score of the participants in the dupilumab clinical trial, which

was used as a reference value to normalize EASI scores in all clinical trials.

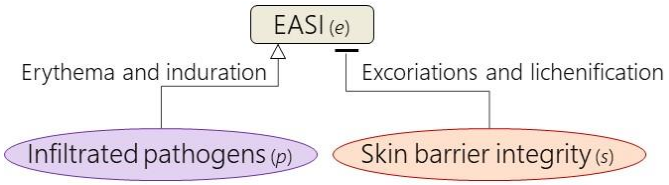

FIGURE S4 Relationship between EASI score and infiltrated pathogens and skin barrier integrity in our model.

We assumed erythema and induration correlate with the infiltrated pathogen load ($p(t)$) because these two signs can be induced by *Staphylococcus aureus*[31], which is commonly colonized in AD skin lesion[32]. Erythema is caused by inflammatory vasodilation by histamines[33]. Histamine is released mainly from mast cells that are activated by detecting infiltrated pathogens as antigens through antigen-specific IgE[34]. Although both infiltrated pathogens and IgE play a role in this process, we associated the released histamine concentration with infiltrated pathogens load in this model because the amount of histamine release is more dependent on the amount of antigens than that of IgE[35]. Low contribution of IgE on the AD pathogenesis is also suggested by a lack of clinical efficacy demonstrated for omalizumab (IgE neutralizing anti-IgE antibody). The other two signs, excoriations and lichenification are caused by scratching[36], which damages skin barrier integrity. The degree of damage of the skin barrier integrity is described by $1 - s(t)$.

The dynamics of $s(t)$ and $p(t)$ that determine $e(t)$ are described below.

(a) Skin barrier integrity

The dynamics of the skin barrier integrity, $s(t)$, is described (FIGURE S5) by

$$\frac{ds(t)}{dt} = \frac{(1-s(t))(k_1 + k_2 c_{22}(t) + k_3)}{(1+b_1 c_4(t))(1+b_2 c_{13}(t))(1+b_3 c_{17}(t))(1+b_4 c_{22}(t))(1+b_5 c_{31}(t))} - s(t)\{d_1(1 + d_3 p(t)) + d_2 c_{31}(t)\}, \quad \text{(S4)}$$

where $c_4(t)$, $c_{13}(t)$, $c_{17}(t)$, $c_{22}(t)$, and $c_{31}(t)$ are the concentrations of IL-4, IL-13, IL-17A, IL-22, and IL-31, respectively, k_1, k_2, and k_3 are the recovery rates of skin barrier integrity via skin turnover, IL-22, and placebo effects, respectively, d_1, d_2, and d_3 are the degradation rates of skin barrier via skin turnover, IL-31, and infiltrated pathogens, respectively, and b_1, b_2, b_3, b_4, and b_5 correspond to the inhibitory strengths for recovery of skin barrier via IL-4, IL-13, IL-17A, IL-22, and IL-31, respectively. Levels of skin barrier integrity were defined between 0 (completely damaged) and 1 (healthy).

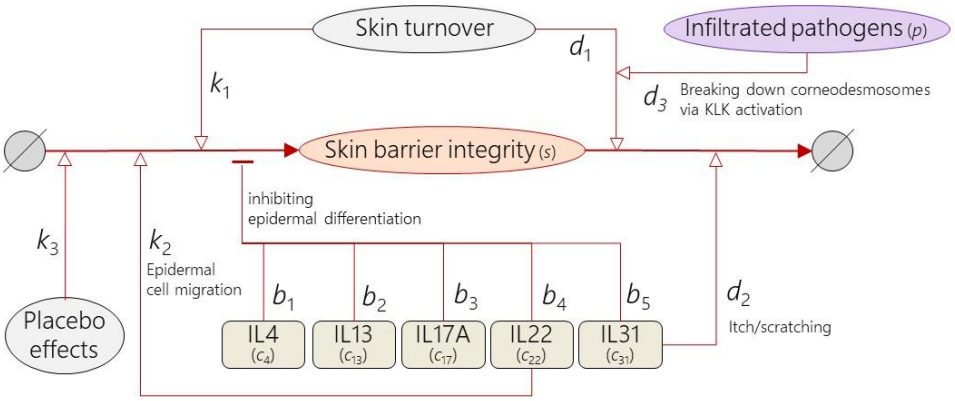

FIGURE S5 Regulation of skin barrier integrity level

Our model assumes that skin barrier integrity recovers by skin turnover (with the recovery rate, k_1), epidermal cell migration (k_2), and placebo effects (k_3). We assumed that skin turnover occurs independently from external perturbation and epidermal cell migration is promoted by IL-22[37]. The placebo effect was applied to the models for both placebo- and drug-treated groups, as placebo-treated patients demonstrated improvement of the EASI score, presumably because of the controlled care for AD patients with concomitant drugs such as emollients in the clinical trials.

We modelled compromise the recovery of skin barrier integrity by IL-4[38] (with the strength b_1), IL-13[39] (b_2), IL-17A[40] (b_3), IL-22[37] (b_4), and IL-31[41] (b_5), as they are shown to decrease filaggrin production and inhibit epidermal differentiation.

We also modelled degradation of the skin barrier by skin turnover (with the degradation rate d_1) and scratching through itch induced by IL-31 (d_2)[42]. Our model assumed that the impairment of skin barrier by skin turnover (d_1) is potentiated by infiltrated pathogens (d_3), such as *Staphylococcus aureus*, as *Staphylococcus aureus* stimulates TLR2[43] and thereby excessively activates KLK5[44] to increase desquamation in the skin turnover process[45].

(b) Infiltrated pathogens

The dynamics of the infiltrated pathogens, $p(t)$, is described (FIGURE S6) by

$$\frac{dp(t)}{dt} = \frac{k_4}{1+b_6 s(t)} - p(t)\left\{\frac{(1+d_4 p(t))(1+d_5 c_{17}(t))(1+d_6 c_{22}(t))(1+d_7 c_g(t))}{(1+b_7 c_4(t))(1+b_8 c_{13}(t))} + d_8\right\}, \qquad \text{(S5)}$$

where k_4 is the rate of pathogen infiltration, d_4, d_5, d_6, d_7, and d_8 are the elimination rates of infiltrated pathogens via infiltrated pathogens themselves, IL-17A, IL-22, IFNg (these factors increase release of AMPs as described below), and skin turnover, respectively, b_6 corresponds to the inhibitory strength for pathogens infiltration via skin barrier, b_7 and b_8 correspond to the inhibitory strengths for elimination of infiltrated pathogens via IL-4 and IL-13, respectively, and $c_g(t)$ is the concentration of IFNg. Levels of the infiltrated pathogens were defined between 0 (pathogen-free) and 1 (maximal infiltration).

We assumed that the steady-state infiltrated pathogen level is 1 (the maximal level of infiltrated pathogens when $\frac{dp(t)}{dt} = 0$) if skin barrier integrity is destructed completely ($s(t) = 0$) and the effects of AMP to decrease infiltrated pathogens is zero ($\frac{(1+d_4 p(t))(1+d_5 c_{17}(t))(1+d_6 c_{22}(t))(1+d_7 c_g(t))}{(1+b_7 c_4(t))(1+b_8 c_{13}(t))} \cong 0$) at the steady-state. This condition leads to $k_4 = d_8$.

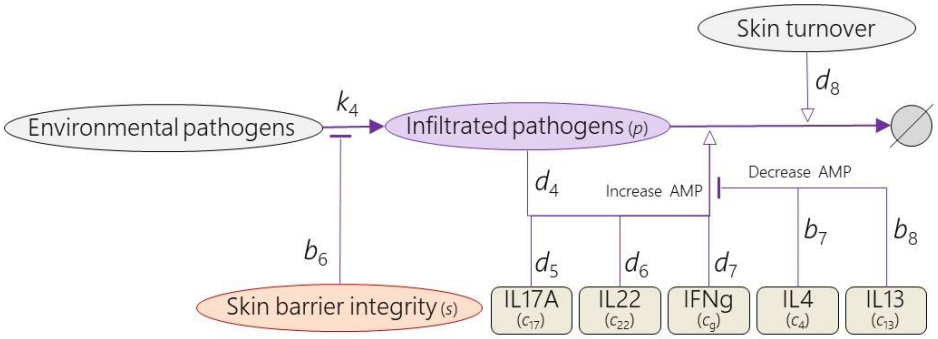

FIGURE S6 Regulation of infiltrated pathogen level

The infiltrated pathogens increase by penetration of environmental pathogens through the skin barrier (with the rate k_4), whose integrity determines how easily pathogens can infiltrate

(with strength b_6). Microbial pathogens are killed by AMP directly[46]. IL-17A[47], IL-22[48], and IFNg[49] increase AMP release from keratinocytes (with the strengths, d_5, d_6 and d_7, respectively), whereas the infiltrated pathogens, such as *Staphylococcus aureus*, also increase AMP release from keratinocytes via other pathways independent to these cytokines[50] (d_4). IL-4 and IL-13 inhibit the AMP release[49] (with the strengths b_7 and b_8). The infiltrated pathogens decrease due to the skin turnover (d_8).

3.2. Cytokines

The dynamics of the cytokines and OX40L, $c_4(t)$, $c_{13}(t)$, $c_{17}(t)$, $c_{22}(t)$, $c_{31}(t)$, $c_{\mathrm{g}}(t)$, $c_{\mathrm{TS}}(t)$, and $c_{\mathrm{OX}}(t)$ are described (FIGURE S7) by

$$\frac{dc_4(t)}{dt} = k_{11}c_{\mathrm{t2}}(t) + k_{12} - d_{10}c_4(t), \quad \text{(S6)}$$

$$\frac{dc_{13}(t)}{dt} = k_{13}c_{\mathrm{t2}}(t) + k_{14} - d_{11}c_{13}(t), \quad \text{(S7)}$$

$$\frac{dc_{17}(t)}{dt} = k_{15}c_{\mathrm{t17}}(t) + k_{16} - d_{12}c_{17}(t), \quad \text{(S8)}$$

$$\frac{dc_{22}(t)}{dt} = k_{17}c_{\mathrm{t22}}(t) + k_{18} - d_{13}c_{22}(t), \quad \text{(S9)}$$

$$\frac{dc_{31}(t)}{dt} = k_{19}c_{\mathrm{t2}}(t) + k_{20} - d_{14}c_{31}(t), \quad \text{(S10)}$$

$$\frac{dc_{\mathrm{g}}(t)}{dt} = k_{21}c_{\mathrm{t1}}(t) + k_{22} - d_{15}c_{\mathrm{g}}(t), \quad \text{(S11)}$$

$$\frac{dc_{\mathrm{TS}}(t)}{dt} = k_{23}p(t) + k_{24} - d_{16}c_{\mathrm{TS}}(t), \quad \text{(S12)}$$

$$\frac{dc_{\mathrm{OX}}(t)}{dt} = k_{25}c_{\mathrm{TS}}(t) + k_{26} - d_{17}c_{\mathrm{OX}}(t), \quad \text{(S13)}$$

where $c_{\mathrm{TS}}(t)$ is the concentrations of TSLP and $c_{\mathrm{OX}}(t)$ is the level of OX40L, k_{11} is the IL-4 secretion rate via Th2 , k_{13} is the IL-13 secretion rate via Th2, k_{15} is the IL-17A secretion rate via Th17, k_{17} is the IL-22 secretion rate via Th22, k_{19} is the IL-31 secretion rate via Th2, k_{21} is are the IFNg secretion rate via Th1, k_{23} is the TSLP secretion rate via infiltrated pathogens, k_{25} is the OX40L expression rate via TSLP, d_{10}, d_{11}, d_{12}, d_{13}, d_{14}, d_{15}, d_{16}, and d_{17} are the elimination rates for IL-4, IL-13, IL-17A, IL-22, IL-31, IFNg, TSLP, and OX40L, respectively, and k_{12}, k_{14}, k_{16}, k_{18}, k_{20}, k_{22}, k_{24}, and k_{26} are the secretion or expression rates of IL-4, IL-13, IL-17A, IL-22, IL-31, IFNg, TSLP, and OX40L via other pathways that were not explicitly considered in the model.

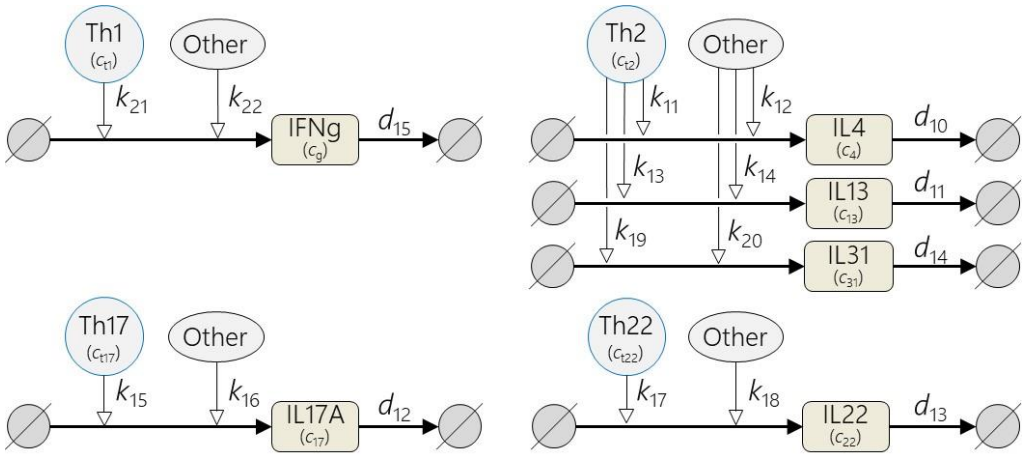

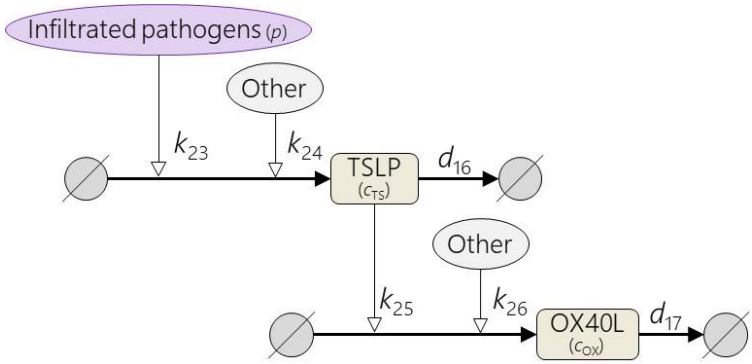

FIGURE S7 Modelling of regulation of cytokine concentrations

Th1 secretes IFNg[51] (with the rate k_{21}), while Th2 secretes IL-4[52], IL-13[51], and IL31[53] (with the rates k_{11}, k_{13}, and k_{19}). Th17 and Th22 produce IL17A[52] and IL-22[54] (with the rates k_{15} and k_{17}). Infiltrated pathogens induce TSLP in keratinocytes through TLR2 pathway[55] (with the rate k_{23}), and TSLP induces DCs to express OX40L[56] (with the rate k_{26}). There are other pathways releasing cytokines, which were implicitly described as "other" effects (with the rates k_{12}, k_{14}, k_{16}, k_{18}, k_{20}, k_{22}, k_{24}, k_{26}).

3.3. T cells

The dynamics of the concentrations of Th1, Th2, Th17, and Th22 cells, $c_{t1}(t)$, $c_{t2}(t)$, $c_{t17}(t)$, and $c_{t22}(t)$, are described (FIGURE S8) by

$$\frac{dc_{t1(t)}}{dt} = k_5 p(t)\left(\frac{1+k_9 c_g(t)}{4+k_9 c_g(t)+k_{10} c_4(t)}\right) - \frac{d_9 c_{t1}(t)}{1+b_9 c_{OX}(t)}, \quad \text{(S14)}$$

$$\frac{dc_{t2}(t)}{dt} = k_6 p(t)\left(\frac{1+k_{10} c_4(t)}{4+k_9 c_g(t)+k_{10} c_4(t)}\right) - \frac{d_9 c_{t2}(t)}{1+b_9 c_{OX}(t)}, \quad \text{(S15)}$$

$$\frac{dc_{t17}(t)}{dt} = k_7 p(t)\left(\frac{1}{4+k_9 c_g(t)+k_{10} c_4(t)}\right) - \frac{d_9 c_{t17}(t)}{1+b_9 c_{OX}(t)}, \quad \text{(S16)}$$

$$\frac{dc_{t22}(t)}{dt} = k_8 p(t)\left(\frac{1}{4+k_9 c_g(t)+k_{10} c_4(t)}\right) - \frac{d_9 c_{t22}(t)}{1+b_9 c_{OX}(t)}, \quad \text{(S17)}$$

where k_5, k_6, k_7, and k_8 are the rates of differentiation of naïve T cells to Th1, Th2, Th17, and Th22, respectively, k_9 and k_{10} are the strengths of polarization for Th1 and Th2 differentiation, respectively, d_9 is the T cell elimination rate, b_9 is the inhibitory strength for T cells elimination by OX40L.

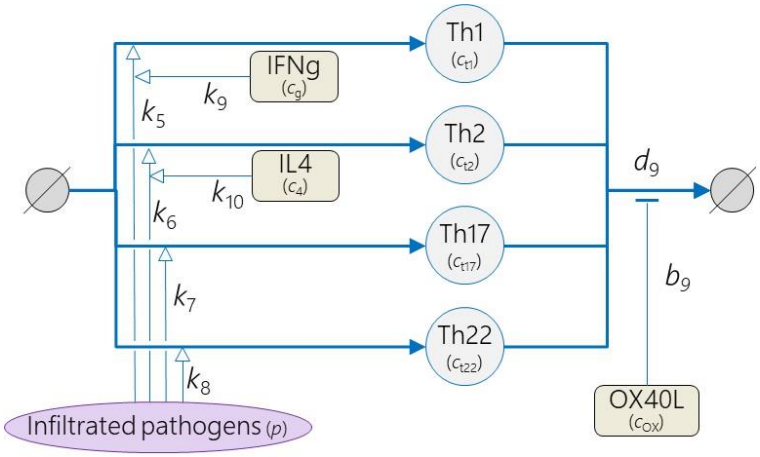

FIGURE S8 Regulation of T-cell concentrations

Concentration of Th1, Th2, Th17, and Th22 cells increases via differentiation of naïve T cells[57] that are primed by dendritic cells (DCs) activated by the infiltrated pathogen[58] (with the rate k_5, k_6, k_7 and k_8, respectively). The balance of the differentiation into each T cell subset depends on the cytokine environment[59]; IFNg drives Th1 polarization[60] (with the strength k_9) while IL-4 promotes differentiation toward Th2[61] (k_{10}). Preferential polarization of certain helper-T cell subset reduces room for other subsets to be differentiated ($\mathrm{Th1}:\mathrm{Th2}:\mathrm{Th17}:\mathrm{Th22} = \left(1+k_9c_\mathrm{g}(t)\right):\left(1+k_{10}c_4(t)\right):1:1$ with ratio to the sum of all the subtypes: $1+k_9c_\mathrm{g}(t)+1+k_{10}c_4(t)+1+1 = 4+k_9c_\mathrm{g}(t)+k_{10}c_4(t)$). The T cells decrease according to their turnover (with the rate d_9). OX40L promotes prolongation of T cell activation and survival (with the strength b_9) as it activates the tumor necrosis factor receptor OX40, and functions as a T-cell costimulatory factor[62].

3.4. Drug effects

We described the effects of the antibodies that inhibit the target signaling by scaling the actual concentrations of the target cytokines or OX40L by an inhibitory rate, r_inhibit, for each drug (Eq. 2 and TABLE S3).

r_inhibit of each drug was defined using the half maximal inhibitory concentration (IC_{50}) of the drug against the target biological factor and the mean concentration of drugs in the skin[63] (d_skin) by

$$r_\mathrm{inhibit} = \begin{cases} \frac{d_\mathrm{skin}}{\mathrm{IC}_{50}+d_\mathrm{skin}}e_{a2}, & \text{if drug is tralokinumab,} \\ \frac{d_\mathrm{skin}}{\mathrm{IC}_{50}+d_\mathrm{skin}}, & \text{otherwise,} \end{cases} \quad \text{(S18)}$$

where e_{a2} represents the inhibitory effects of IL-13 binding to IL-13Rα2 in tralokinumab. d_skin is defined by $r_\mathrm{skin/serum}d_\mathrm{serum}$, where $r_\mathrm{skin/serum}$ is a ratio of drug concentration in the skin to that in serum and d_serum is the mean concentration of the drug in serum. We adopted $r_\mathrm{skin/serum} = 0.157$ for all the antibodies based on the estimated ratio of antibody concentration in the skin to that in the plasma[64]. Values of IC_{50} and d_serum (TABLE S3) were obtained from reported results of in vitro assay and the reported pharmacokinetics data of the adopted dose regimen (TABLE 1) in clinical trials.

We introduced e_{a2} for tralokinumab because tralokinumab not only inhibits IL-13 signaling via IL-13Rα1 but also enhances IL-13 signaling via inhibition of IL-13 binding to IL-13Rα2. IL-13Rα1 forms a heterodimeric receptor with IL-4Rα and is related to the effects of IL-13 signaling in AD pathogenesis. IL-13Rα2 is a decoy receptor to decrease IL-13 signaling via IL-13Rα1. Hence, the influence of the inhibition of IL-13Rα2 in tralokinumab was described by e_{a2} to scale down the r_inhibit based on the IC_{50} against IL-13Rα1. On the other hand, lebrikizumab prevents IL-13 from binding to IL-13Rα1 only[65]. We adopted $e_{a2} = 0.44$ so that it reproduces the differences of %improved EASI and EASI-75 between tralokinumab and lebrikizumab (FIGURE 3).

We also described the effects of rIFNg that replaces the target cytokine (IFNg) by estimating the mean concentration, c_rIFNg, of rIFNg in the skin (TABLE S3). c_rIFNg was estimated using the reported mean concentration of IFNg in the serum after rIFNg administration and the estimated ratio of rIFNg concentration in the skin to that in the plasma[66] by

$$c_{\mathrm{rIFNg}} = \frac{r_{\mathrm{IFNg\_skin/serum}} d_{\mathrm{rIFNg\_serum}}}{d_{\mathrm{IFNg\_skin}}}, \quad \text{(S19)}$$

where $d_{\mathrm{rIFNg\_serum}}$ is the mean concentration of rIFNg in serum after the rIFNg administration (i.e., the increased concentration of IFNg), $r_{\mathrm{IFNg\_skin/serum}}$ and $d_{\mathrm{IFNg\_skin}}$ are a ratio of rIFNg concentration in the skin to that in serum and mean concentration of IFNg in the skin in the observational study, respectively. $d_{\mathrm{rIFNg\_serum}}$ and $d_{\mathrm{IFNg\_skin}}$ were obtained from the pharmacokinetics data of rIFNg[67] and the IFNg concentration in the healthy skin in the observational study[68], respectively. We adopted $r_{\mathrm{IFNg\_skin/serum}} = 1.60$ based on the estimated ratio of macromolecule concentration in the skin to that in the plasma[66].

TABLE S3 Parameter values for effects of drugs used in this study

Drugs	IC_{50} (mcg/mL)	$d_{\mathrm{skin}}/d_{\mathrm{serum}}$ or $d_{\mathrm{rIFNg\_skin}}/d_{\mathrm{rIFNg\_serum}}$ (mcg/mL)	r_{inhibit}							c_{rIFNg} (fold change against healthy skin)
			IL-4	IL-13	IL-17A	IL-22	IL-31	TSLP	OX40L	IFNg
Dupilumab[69, 70]	IL-4: <0.01 IL-13: 0.01	183/29	0.99	0.99	-	-	-	-	-	-
Nemolizumab[71,72]	0.01	6/1	-	-	-	-	0.99	-	-	-
Tezepelumab[73, 74]	0.21	109/17	-	-	-	-	-	0.99	-	-
GBR 830[75, 76]	0.13	90/14	-	-	-	-	-	-	0.99	-
Fezakinumab[a]	-	-	-	-	-	0.99	-	-	-	-
Secukinumab[77,78]	0.08	45/7	-	-	0.99	-	-	-	-	-
Tralokinumab[65, 79]	0.10	70/11	-	$0.99e_{a2}$	-	-	-	-	-	-
Lebrikizumab[80 b]	0.10	91/14	-	0.99	-	-	-	-	-	-
rIFNg[67]	-	4.0E-6 /5.3E-4	-	-	-	-	-	-	-	2.1E2

a: IC_{50} and mean concentration were not found in published literature. We assumed an almost complete inhibition (the 99% inhibition as the same as other antibodies) for fezakinumab. b: IC_{50} and mean concentration were not found in the publication. We assumed that tralokinumab and lebrikizumab have the equivalent IC_{50} because their mechanisms of binding are similar[65] and that the mean drug concentration of 250 mg q2w is four times larger than that of 125 mg q4w (reported mean drug concentration is 22.8 mcg/mL).

4. Model parameters

We selected 102 parameters of the distributions (μ_n and σ_n that define the distributions of the 51 parameters, TABLE S4) by

1) calculating μ_n of elimination rates for 11 biological factors based on available data and assumptions, and

2) tuning the remaining 91 parameter values so that the model reproduces clinical data.

TABLE S4 Optimal parameter values obtained by parameter tuning

Parameters		μ_n	σ_n	Comments
k_1	Recovery rate of skin barrier integrity via skin turnover	0.54	0.79	-
k_2	Recovery rate of skin barrier integrity via IL-22	-1.50	0.39	-
k_3	Recovery rate of skin barrier integrity via placebo effects	2.95	1.42	-
k_4	Rate of pathogen infiltration	-	-	$k_4 = d_8$ (Section S3.1 (b))
k_5	Rate of differentiation of naïve T cells to Th1	2.95	0.04	-
k_6	Rate of differentiation of naïve T cells to Th2	3.89	0.00	-
k_7	Rate of differentiation of naïve T cells to Th17	2.60	0.07	-
k_8	Rate of differentiation of naïve T cells to Th22	4.83	0.48	-
k_9	Strength of polarization for Th1 differentiation	-3.32	0.99	-
k_{10}	Strength of polarization for Th2 differentiation	-5.82	0.07	-
k_{11}	IL-4 secretion rate via Th2	5.50	0.16	-
k_{12}	IL-4 secretion rate via other pathways	9.25	0.51	-
k_{13}	IL-13 secretion rate via Th2	6.65	0.37	-
k_{14}	IL-13 secretion rate via other pathways	8.84	0.45	-
k_{15}	IL-17A secretion rate via Th17	4.01	0.27	-
k_{16}	IL-17A secretion rate via other factors	2.64	0.85	-
k_{17}	IL-22 secretion rate via Th22	1.19	0.21	-
k_{18}	IL-22 secretion rate via other factors	1.46	0.03	-
k_{19}	IL-31 secretion rate via Th2	1.54	0.19	-
k_{20}	IL-31 secretion rate via other factors	1.99	0.58	-
k_{21}	IFNg secretion rate via Th1	0.46	1.00	-
k_{22}	IFNg secretion rate via other factors	2.62	0.35	-
k_{23}	TSLP secretion rate via infiltrated pathogens	4.00	0.52	-
k_{24}	TSLP secretion rate via other factors	4.43	0.65	-
k_{25}	OX40L expression rates via TSLP	0.42	0.48	-
k_{26}	OX40L expression rates via other factors	1.68	0.78	-
b_1	Inhibitory strength for recovery of skin barrier via IL-4	-8.69	0.57	-
b_2	Inhibitory strength for recovery of skin barrier via IL-13	-3.54	1.58	-
b_3	Inhibitory strength for recovery of skin barrier via IL-17	-3.92	0.35	-
b_4	Inhibitory strength for recovery of skin barrier via IL-22	-0.59	0.80	-
b_5	Inhibitory strength for recovery of skin barrier via IL-31	-2.09	0.90	-
b_6	inhibitory strength for pathogens infiltration via skin barrier	0.39	0.44	-
b_7	Inhibitory strength for elimination of infiltrated pathogens via IL-4	-7.99	0.09	-
b_8	Inhibitory strength for elimination of infiltrated pathogens via IL-13	-3.50	0.05	-
b_9	Inhibitory strength for T cells elimination by OX40L	-2.66	0.30	-
d_1	Degradation rate of skin barrier via skin turnover	-1.60	1.53	μ_n based on half-live (TABLE S5)
d_2	Degradation rate of skin barrier via IL-31	-2.64	0.57	-
d_3	Degradation rate of skin barrier via infiltrated pathogens	1.25	2.28	-
d_4	Elimination rate of infiltrated pathogens via infiltrated pathogens themselves	-1.00	0.47	-
d_5	Elimination rate of infiltrated pathogens via IL-17A	-5.10	0.45	-
d_6	Elimination rate of infiltrated pathogens via IL-22	-5.01	0.39	-
d_7	Elimination rate of infiltrated pathogens via IFNg	-8.70	0.62	-
d_8	Elimination rate of infiltrated pathogens via skin turnover	-1.60	0.04	μ_n based on half-live (TABLE S5)
d_9	T cell elimination rate	-0.55	0.09	μ_n based on half-live (TABLE S5)
d_{10}	Elimination rates for IL-4	5.91	0.22	μ_n based on half-live (TABLE S5)
d_{11}	Elimination rates for IL-13	5.91	0.11	μ_n based on half-live (TABLE S5)
d_{12}	Elimination rates for IL-17A	3.33	0.57	μ_n based on half-live (TABLE S5)
d_{13}	Elimination rates for IL-22	3.33	0.56	μ_n based on half-live (TABLE S5)
d_{14}	Elimination rates for IL-31	3.33	0.10	μ_n based on half-live (TABLE S5)
d_{15}	Elimination rates for IFNg	2.68	0.15	μ_n based on half-live (TABLE S5)
d_{16}	Elimination rates for TSLP	3.33	0.20	μ_n based on half-live (TABLE S5)
d_{17}	Elimination rates for OX40L	0.48	0.24	μ_n based on half-live (TABLE S5)

4.1. μ_n of elimination rates calculated with published data and assumptions

The elimination rates of the 11 biological factors were determined using the half-lives measured in vivo (serum) in humans (TABLE S5). The calculated values were set as the μ_n,

the mean value for each distribution.

TABLE S5 Elimination rates of biological factors used in this study

Parameters	Biological factors	Elimination rate (/week)	Half-life (week)	Comments on half-lives
d_1	Skin barrier integrity	0.202	3.4[81]	Based on the half-life of the epidermis
d_8	Infiltrated pathogens	0.202	3.4[81]	Based on the half-life of the epidermis
d_9	Th1	0.578	1.2[82]	-
	Th2			
	Th17			
	Th22			
d_{10}	IL-4	368	1.9E-03[83]	-
d_{11}	IL-13	368	1.9E-03	Assumed same as IL-4 because IL-4 and IL-13 are the same IL-2 sub-family
d_{12}	IL-17A	28.0	2.5E-02	Assumed mean value of IL-4 and IFNg as average cytokine
d_{13}	IL-22	28.0	2.5E-02	Assumed mean value of IL-4 and IFNg as average cytokine
d_{14}	IL-31	28.0	2.5E-02	Assumed mean value of IL-4 and IFNg as average cytokine
d_{15}	IFNg	14.6	4.8E-02[84]	-
d_{16}	TSLP	28.0	2.5E-02	Assumed mean value of IL-4 and IFNg as average cytokine
d_{17}	OX40L	1.62	0.4[85]	Based on dendritic cells of mouse data. OX40L are expressed on dendritic cells.

4.2. Parameters tuned to reproduce clinical data

The remaining 91 parameters were tuned so that the model reproduces the following clinical data consisting of 136 reference values;

- mean values and coefficient of variation (%CV) of 12 biological factors (IL-4, IL-13, IL-17A, IL-22, IL-31, IFNg, TSLP, OX40L, Th1, Th2, Th17, and Th22) in observational studies and baseline EASI score in clinical trial of dupilumab (TABLE S2. 2 indices x 13 factors = 26 reference values) and
- mean EASI score and EASI-75 when 9 drugs and placebo were applied in clinical trials (FIGURE 1. 2 indices x 10 interventions x 1-10 time points/intervention = 110 reference values).

We searched the parameters that minimizes the cost function, ***J***, defined by

$$\boldsymbol{J} = w_1 J_1 + w_2 J_2 + w_3 J_3 + w_4 J_4, \tag{S18}$$

where

$$J_1 = \sqrt{\frac{1}{l}\sum_{h=1}^{l}(u_h - \hat{u}_h)^2}, \tag{S19}$$

$$J_2 = \sqrt{\frac{1}{l}\sum_{h=1}^{l}(v_h - \hat{v}_h)^2}, \tag{S20}$$

$$J_3 = \sqrt{\frac{1}{n}\sum_{i=1}^{n}\left\{\frac{1}{m}\sum_{j=1}^{m} w_{\mathrm{T}}\left(a_i(t_j) - \hat{a}_i(t_j)\right)\right\}^2}, \tag{S21}$$

$$J_4 = \sqrt{\frac{1}{n}\sum_{i=1}^{n}\left\{\frac{1}{m}\sum_{j=1}^{m} w_{\mathrm{T}}\left(b_i(t_j) - \hat{b}_i(t_j)\right)\right\}^2}. \tag{S22}$$

The terms, J_1 and J_2 are root mean squared errors of mean values and %CV of biological factors, respectively. J_3 and J_4 are weighted root mean squared errors of mean EASI score

and EASI-75, respectively. w_1 to w_4 are the weighting coefficients. u_h and v_h are the mean value and the %CV of the *h*-th biological factor (*h*=1, …, *I*) in the observational studies. $\hat{u}_h$ and $\hat{v}_h$ are the corresponding values among 1000 virtual patients in the simulation at the steady-state (after 1000 weeks). $a_i(t_j)$ and $b_i(t_j)$ are the reference value of the mean EASI score and of EASI-75 in the study using the *i*-th drug (*i*=1, …, *n*) at time t_j (*j*=1,…,*m*) with the weighting for time points, w_{T} . $\hat{a}_i(t_j)$ and $\hat{b}_i(t_j)$ are the corresponding simulated values. We used $(w_1, w_2, w_3, w_4) = (10,1,1,1)$ and $w_{\mathrm{T}} = \begin{cases} 1 & (t_j < 8) \\ 10 & (t_j \geq 8) \end{cases}$. We set a higher weight on the mean values of the biological factors, w_1, because its fitting error tends to be smaller than other items (ie, %CV of the biological factors, the mean EASI score, and EASI-75). We also set a higher weight on the time points of 8 weeks or later, w_{T}, because the efficacies are evaluated at least after 8 weeks as primary endpoints in the clinical trials[86].

Parameter tuning was based on differential evolution[87], which is known to be an effective method for global optimization of a large number of parameters. The conditions for differential evolution were set as follows based on manual trial-and-error.

Mutation constant (F)	: 0.5
Crossover constant (CR)	: 0.7
Strategy	: DE/best/1/bin
Number of population vectors (NP)	: 92
Number of function evaluations (nfe)	: 46092
Ranges of parameters searched	: TABLE S6

We tuned both the 91 parameters of the distributions and e_{a2} (92 parameters in total) at once. ***J*** was minimized to 27.1, where the model fitness was confirmed visually (FIGURE 3).

As reference information, we also calculated (not-weighted) root mean squared errors of mean EASI score and EASI-75 by

$$J_5 = \sqrt{\frac{1}{n}\sum_{i=1}^{n}\left\{\frac{1}{m}\sum_{j=1}^{m}\left(a_i(t_j) - \hat{a}_i(t_j)\right)\right\}^2}, \quad \text{(S23)}$$

$$J_6 = \sqrt{\frac{1}{n}\sum_{i=1}^{n}\left\{\frac{1}{m}\sum_{j=1}^{m}\left(b_i(t_j) - \hat{b}_i(t_j)\right)\right\}^2}. \quad \text{(S24)}$$

TABLE S6 Ranges of parameters searched in parameter tuning

Parameters		μ_n	σ_n	Comments
k_1	Recovery rate of skin barrier integrity via skin turnover	[0, 1]	[0, 1]	-
k_2	Recovery rate of skin barrier integrity via IL-22	[-2, -1]	[0, 1]	-
k_3	Recovery rate of skin barrier integrity via placebo effects	[2, 3]	[1, 2]	-
k_4	Rate of pathogen infiltration	-	-	$k_4 = d_8$ (Section S3.1 (b))
k_5	Rate of differentiation of naïve T cells to Th1	[2, 3]	[0, 1]	-
k_6	Rate of differentiation of naïve T cells to Th2	[3, 4]	[0, 1]	-
k_7	Rate of differentiation of naïve T cells to Th17	[2, 3]	[0, 1]	-
k_8	Rate of differentiation of naïve T cells to Th22	[4, 5]	[0, 1]	-
k_9	Strength of polarization for Th1 differentiation	[-4, -3]	[0, 1]	-
k_{10}	Strength of polarization for Th2 differentiation	[-6, -5]	[0, 1]	-
k_{11}	IL-4 secretion rate via Th2	[5, 6]	[0, 1]	-
k_{12}	IL-4 secretion rate via other pathways	[9, 10]	[0, 1]	-
k_{13}	IL-13 secretion rate via Th2	[6, 7]	[0, 1]	-
k_{14}	IL-13 secretion rate via other pathways	[8, 9]	[0, 1]	-
k_{15}	IL-17A secretion rate via Th17	[4, 5]	[0, 1]	-
k_{16}	IL-17A secretion rate via other factors	[2, 3]	[0, 1]	-
k_{17}	IL-22 secretion rate via Th22	[1, 2]	[0, 1]	-
k_{18}	IL-22 secretion rate via other factors	[1, 2]	[0, 1]	-
k_{19}	IL-31 secretion rate via Th2	[1, 2]	[0, 1]	-
k_{20}	IL-31 secretion rate via other factors	[1, 2]	[0, 1]	-
k_{21}	IFNg secretion rate via Th1	[0, 1]	[1, 2]	-
k_{22}	IFNg secretion rate via other factors	[2, 3]	[0, 1]	-
k_{23}	TSLP secretion rate via infiltrated pathogens	[4, 5]	[0, 1]	-
k_{24}	TSLP secretion rate via other factors	[4, 5]	[0, 1]	-
k_{25}	OX40L expression rates via TSLP	[0, 1]	[0, 1]	-
k_{26}	OX40L expression rates via other factors	[1, 2]	[0, 1]	-
b_1	Inhibitory strength for recovery of skin barrier via IL-4	[-9, -8]	[0, 1]	-
b_2	Inhibitory strength for recovery of skin barrier via IL-13	[-4, -3]	[1, 2]	-
b_3	Inhibitory strength for recovery of skin barrier via IL-17	[-4, -3]	[0, 1]	-
b_4	Inhibitory strength for recovery of skin barrier via IL-22	[-1, 0]	[0, 1]	-
b_5	Inhibitory strength for recovery of skin barrier via IL-31	[-3, -2]	[0, 1]	-
b_6	inhibitory strength for pathogens infiltration via skin barrier	[0, 1]	[0, 1]	-
b_7	Inhibitory strength for elimination of infiltrated pathogens via IL-4	[-8, -7]	[0, 1]	-
b_8	Inhibitory strength for elimination of infiltrated pathogens via IL-13	[-4, -3]	[0, 1]	-
b_9	Inhibitory strength for T cells elimination by OX40L	[-3, -2]	[0, 1]	-
d_1	Degradation rate of skin barrier via skin turnover	-	[1, 2]	μ_n based on half-live (TABLE S5)
d_2	Degradation rate of skin barrier via IL-31	[-3, -2]	[0, 1]	
d_3	Degradation rate of skin barrier via infiltrated pathogens	[1, 2]	[2, 3]	-
d_4	Elimination rate of infiltrated pathogens via infiltrated pathogens themselves	[-2, -1]	[0, 1]	-
d_5	Elimination rate of infiltrated pathogens via IL-17A	[-6, -5]	[0, 1]	-
d_6	Elimination rate of infiltrated pathogens via IL-22	[-6, -5]	[0, 1]	-
d_7	Elimination rate of infiltrated pathogens via IFNg	[-9, -8]	[0, 1]	-
d_8	Elimination rate of infiltrated pathogens via skin turnover	-	[0, 1]	μ_n based on half-live (TABLE S5)
d_9	T cell elimination rate	-	[0, 1]	μ_n based on half-live (TABLE S5)
d_{10}	Elimination rates for IL-4	-	[0, 1]	μ_n based on half-live (TABLE S5)
d_{11}	Elimination rates for IL-13	-	[0, 1]	μ_n based on half-live (TABLE S5)
d_{12}	Elimination rates for IL-17A	-	[0, 1]	μ_n based on half-live (TABLE S5)
d_{13}	Elimination rates for IL-22	-	[0, 1]	μ_n based on half-live (TABLE S5)
d_{14}	Elimination rates for IL-31	-	[0, 1]	μ_n based on half-live (TABLE S5)
d_{15}	Elimination rates for IFNg	-	[0, 1]	μ_n based on half-live (TABLE S5)
d_{16}	Elimination rates for TSLP	-	[0, 1]	μ_n based on half-live (TABLE S5)
d_{17}	Elimination rates for OX40L	-	[0, 1]	μ_n based on half-live (TABLE S5)

5. Influences of pathophysiological backgrounds of virtual patients on clinical efficacy

We investigated the influence of the 51 model parameters on %improve EASI of each drug using the LHS-PRCC (FIGURE 4), and simulated the %improve EASI at week 24 after patient stratification based on the baseline levels of cytokines in the skin (FIGURE S9) with regards to drugs other than dupilumab as well.

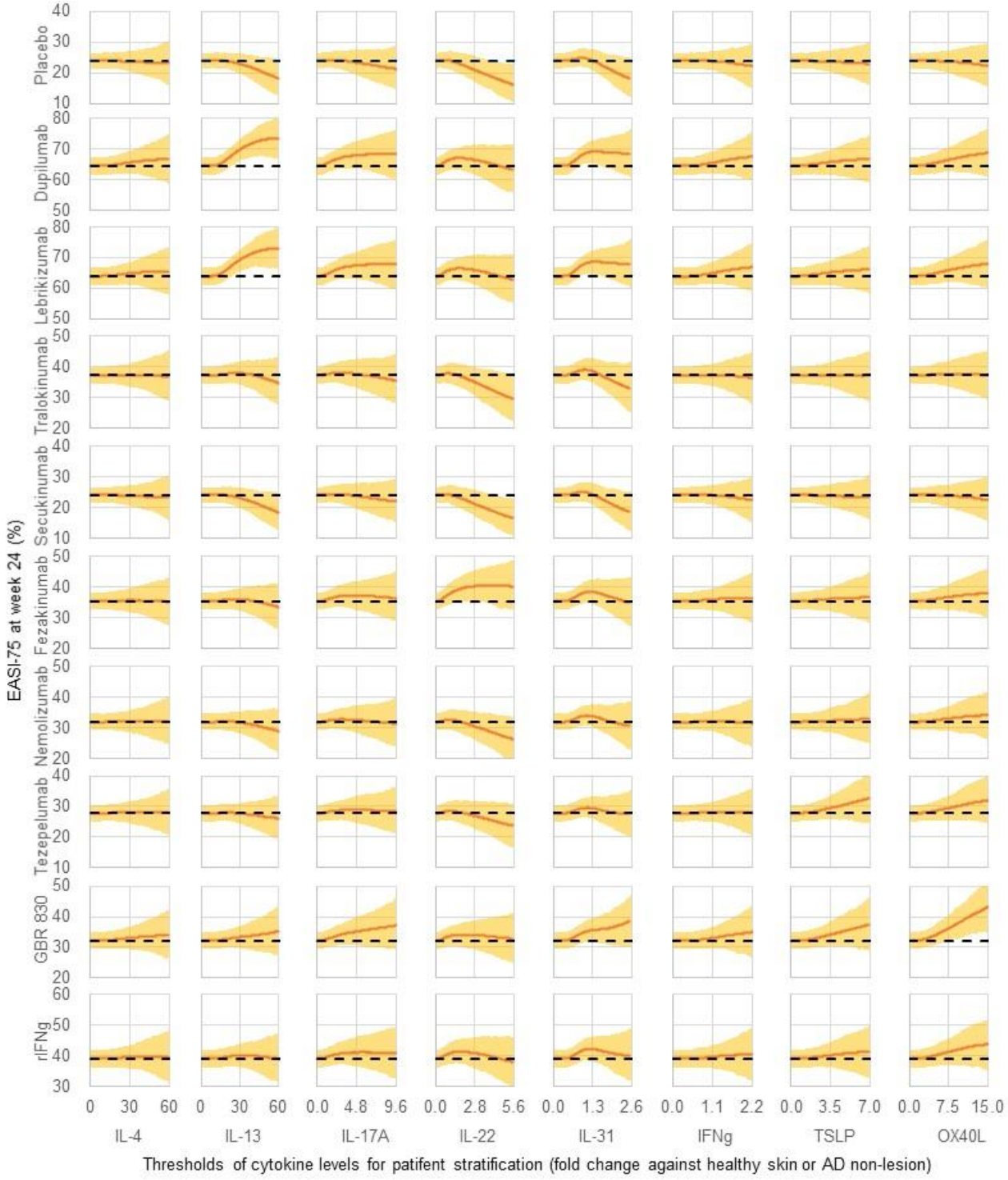

FIGURE S9 Simulated EASI-75 at 24 weeks after drug treatment (y-axis) for stratified patients with their cytokine baseline levels larger than the threshold values (x-axis)

The number of stratified virtual patients decreases for a larger threshold value. The threshold of zero includes all the virtual patients and the maximum threshold value corresponds to inclusion of at least 10% of 1000 virtual patients, who were generated according to the tuned distributions of the parameters (TABLE S4). Simulation was iterated 1000 times where a cohort of 1000 virtual patients were created at each iteration. Lines and

shaded areas are the mean value and 95% CI of 1000 simulations, respectively. The higher EASI-75 compared with that without patient stratification (with the threshold value of zero: dashed line) suggests a success in stratifying good responders.

5.1. Influence of skin barrier on placebo effects

Three skin barrier-related parameters (k_1, k_3, and b_6) had a significant PRCC with the efficacy in placebo group (FIGURE 4); these influences were also observed in all the drugs as the placebo effects were considered in both placebo- and drug-treated groups in the simulation.

The virtual patients with a lower k_1 and a higher k_3 benefited more from recovery of skin barrier via placebo effects, and thereby achieved a higher %improve EASI. The virtual patients with a higher b_6 inhibit pathogen infiltration more strongly through the recovery of skin barrier by placebo effects, and thereby achieved higher %improve EASI. These results may suggest that older patients whose skin has a slow baseline turnover (a lower k_1) but can inhibit pathogen infiltration (a higher b_6, e.g., sufficient filaggrin functions to form skin barrier) are more responsive to placebo effects.

5.2. Influence of skin barrier on efficacy in multiple drugs in common

Four skin barrier-related parameters (b_2, b_4, d_1, and d_3) had a significant PRCC with the %improved EASI by several drugs (FIGURE 4). These influences correspond to baseline severity of skin barrier defects rather than MoA of each drug.

Virtual patients with higher b_2, b_4, d_1, and d_3 were more responsive to treatment by several drugs (i.e., dupilumab, lebrikizumab, fezakinumab, and rIFNg) because they benefit from recovery of skin barrier via each drug MoA, achieving a higher %improve EASI. These results suggest that patients with a higher degradation rate of skin barrier via skin turnover (d_1, e.g., activity of kallikreins to degrade skin barrier) and via infiltrated pathogens (d_3, e.g., amounts of extracellular protease from S. aureus to degrade skin barrier), as well as a larger influence of cytokines on skin barrier damage (b_2 and b_4 correspond to IL-13 and IL-22), are more responsive to several drugs.

5.3. Influence of IL-13 level on efficacy in lebrikizumab and tralokinumab

The results for lebrikizumab and tralokinumab were similar to those about dupilumab as both drugs have the drug target IL-13 in common, although tralokinumab was less influenced by the IL-13-related parameters due to the lower inhibition rate of IL-13 than lebrikizumab (estimated 44% of lebrikizumab: $e_{\mathrm{a}2} = 0.44$).

Ten model parameters had a significant PRCC with the %improved EASI by lebrikizumab (FIGURE 4). Four out of the ten parameters are IL-13-related (k_{13}, k_{14}, b_2, and d_{11}), and the remaining six parameters are skin barrier-related parameters (k_1, k_3, b_4, b_6 d_1, and d_3) that correspond to placebo effects and baseline severity of skin barrier defects rather than MoA of lebrikizumab.

The four IL-13 related parameters (k_{13}, k_{14}, b_2, and d_{11}) characterize responders for lebrikizumab. Virtual patients with higher k_{13}, k_{14}, and b_2 and a lower d_{11} were more responsive to treatment by lebrikizumab. The parameters, k_{13}, k_{14}, and d_{11}, affect the IL-13 baseline level, and EASI-75 was improved by stratifying virtual patients with a higher IL-13 baseline level (FIGURE S9). The parameter, b_2, describes the influence of IL-13 on skin barrier damage.

Four model parameters had a significant PRCC with the %improved EASI by tralokinumab (FIGURE 4). One out of the six parameters are IL-13-related (b_2), and the remaining five parameters are skin barrier-related parameters (k_1, k_3, and b_6) that correspond to placebo effects rather than MoA of tralokinumab.

Virtual patients with higher b_2 were more responsive to treatment by tralokinumab, although the extent was smaller than the case of lebrikizumab. As opposed to lebrikizumab, EASI-75 was not improved by stratifying virtual patients with a higher IL-13 baseline level (FIGURE S8).

5.4. Influence of IL-22 level on efficacy in fezakinumab

Eight model parameters had a significant PRCC with the %improved EASI by fezakinumab (FIGURE 4). Two out of the eight parameters are IL-22-related (b_4 and d_{13}), and the remaining six parameters are skin barrier-related parameters (k_1, k_3, b_2, b_6 d_1, and d_3) that correspond to placebo effects and baseline severity of skin barrier defects rather than MoA of fezakinumab.

The two IL-22-related parameters (b_4 and d_{13}) can characterize responders for fezakinumab as virtual patients with lower d_{13} were more responsive to treatment by fezakinumab. The parameter, d_{13}, affect the IL-22 baseline level, and EASI-75 was slightly improved by stratifying virtual patients with a higher IL-22 baseline level (FIGURE S9). It is consistent with the results from actual clinical trials of fezakinumab, where a higher efficacy was observed in the AD patients with higher baseline mRNA levels of IL-22[88]. The parameter, b_4, describes the influence of IL-22 on skin barrier damage.

5.5. Influence of Th1 polarization on efficacy in rIFNg

Eight model parameters had a significant PRCC with the %improved EASI by rIFNg (FIGURE 4). One out of the nine parameters is strength of polarization for Th1 differentiation (k_9), which is related to IFNg (i.e., IFNg drives Th1 polarization), and the remaining seven parameters are skin barrier-related parameters (k_1, k_3, b_2, b_4, b_6, d_1, and d_3) that correspond to placebo effects and baseline severity of skin barrier defects rather than MoA of rIFNg. There was no improvement in EASI-75 by stratifying virtual patients with any cytokine baseline level (FIGURE S9).

6. References

1. Iyengar SR, Hoyte EG, Loza A, et al. Immunologic effects of omalizumab in children with severe refractory atopic dermatitis: a randomized, placebo-controlled clinical trial. Int Arch Allergy Immunol. 2013;162(1):89-93
2. Heil PM, Maurer D, Klein B, Hultsch T, Stingl G. Omalizumab therapy in atopic dermatitis: depletion of IgE does not improve the clinical course - a randomized, placebo-controlled and double blind pilot study. J Dtsch Dermatol Ges. 2010;8(12):990-998
3. Kang EG, Narayana PK, Pouliquen IJ, Lopez MC, Ferreira-Cornwell MC, Getsy JA. Efficacy and safety of mepolizumab administered subcutaneously for moderate to severe atopic dermatitis. Allergy. 2020;75(4):950-953
4. Oldhoff JM, Darsow U, Werfel T, et al. Anti-IL-5 recombinant humanized monoclonal antibody (mepolizumab) for the treatment of atopic dermatitis. Allergy. 2005;60(5):693-696
5. MorphoSys AG: Ad hoc: MOR106 Clinical Development in Atopic Dermatitis Stopped for Futility. https://www.morphosys.com/media-investors/media-center/morphosys-ag-ad-hoc-mor106-clinical-development-in-atopic-dermatitis (Accessed on 2021 Feb 6).
6. AnaptysBio. “Corporate overview” J.P. Morgan 38th Annual Healthcare Conference. January 2020. https://sec.report/Document/0001370053-20-000003/a1152020exhibit991.htm
7. Navarini AA, French LE, Hofbauer GF. Interrupting IL-6-receptor signaling improves atopic dermatitis but associates with bacterial superinfection. J Allergy Clin Immunol. 2011;128(5):1128-1130
8. Saeki H, Kabashima K, Tokura Y, et al. Efficacy and safety of ustekinumab in Japanese patients with severe atopic dermatitis: a randomized, double-blind, placebo-controlled, phase II study. Br J Dermatol. 2017;177(2):419-427
9. Khattri S, Brunner PM, Garcet S, et al. Efficacy and safety of ustekinumab treatment in adults with moderate-to-severe atopic dermatitis. Exp Dermatol. 2017;26(1):28-35
10. Jacobi A, Antoni C, Manger B, Schuler G, Hertl M. Infliximab in the treatment of moderate to severe atopic dermatitis. J Am Acad Dermatol. 2005;52(3 Pt 1):522-526
11. Cassano N, Loconsole F, Coviello C, Vena GA. Infliximab in recalcitrant severe atopic eczema associated with contact allergy. Int J Immunopathol Pharmacol. 2006;19(1):237-240
12. Rullan P, Murase J. Two cases of chronic atopic dermatitis treated with soluble tumor necrosis factor receptor therapy. J Drugs Dermatol. 2009;8(9):873-876
13. Buka RL, Resh B, Roberts B, Cunningham BB, Friedlander S. Etanercept is minimally effective in 2 children with atopic dermatitis. J Am Acad Dermatol. 2005;53(2):358-359
14. Simon D, Hösli S, Kostylina G, Yawalkar N, Simon HU. Anti-CD20 (rituximab) treatment improves atopic eczema. J Allergy Clin Immunol. 2008;121(1):122-128
15. Sedivá A, Kayserová J, Vernerová E, et al. Anti-CD20 (rituximab) treatment for atopic eczema. J Allergy Clin Immunol. 2008;121(6):1515-1517
16. McDonald BS, Jones J, Rustin M. Rituximab as a treatment for severe atopic eczema: failure to improve in three consecutive patients. Clin Exp Dermatol. 2016;41(1):45-47
17. Ungar B, Pavel AB, Li R, et al. Phase 2 randomized, double-blind study of IL-17 targeting with secukinumab in atopic dermatitis. J Allergy Clin Immunol. 2021;147(1):394-397
18. Simpson EL, Parnes JR, She D, et al. Tezepelumab, an anti-thymic stromal lymphopoietin monoclonal antibody, in the treatment of moderate to severe atopic dermatitis: A randomized phase 2a clinical trial. J Am Acad Dermatol. 2019;80(4):1013-

1021
19. Guttman-Yassky E, Pavel AB, Zhou L, et al. GBR 830, an anti-OX40, improves skin gene signatures and clinical scores in patients with atopic dermatitis. J Allergy Clin Immunol. 2019;144(2):482-493.e7
20. Hanifin JM, Schneider LC, Leung DY, et al. Recombinant interferon gamma therapy for atopic dermatitis. J Am Acad Dermatol. 1993;28(2 Pt 1):189-197
21. Wang EB, Shen L, Heathman M, Chan JR. Incorporating Placebo Response in Quantitative Systems Pharmacology Models. CPT Pharmacometrics Syst Pharmacol. 2019;8(6):344-346
22. Kabashima K, Matsumura T, Komazaki H, Kawashima M; Nemolizumab-JP01 Study Group. Trial of Nemolizumab and Topical Agents for Atopic Dermatitis with Pruritus. N Engl J Med. 2020;383(2):141-150
23. Guttman-Yassky E, Blauvelt A, Eichenfield LF, et al. Efficacy and Safety of Lebrikizumab, a High-Affinity Interleukin 13 Inhibitor, in Adults With Moderate to Severe Atopic Dermatitis: A Phase 2b Randomized Clinical Trial. JAMA Dermatol. 2020;156(4):411-420
24. Koppes SA, Brans R, Ljubojevic Hadzavdic S, Frings-Dresen MH, Rustemeyer T, Kezic S. Stratum Corneum Tape Stripping: Monitoring of Inflammatory Mediators in Atopic Dermatitis Patients Using Topical Therapy. Int Arch Allergy Immunol. 2016;170(3):187-193
25. Szegedi K, Lutter R, Res PC, et al. Cytokine profiles in interstitial fluid from chronic atopic dermatitis skin. J Eur Acad Dermatol Venereol. 2015;29(11):2136-2144
26. Sano Y, Masuda K, Tamagawa-Mineoka R, et al. Thymic stromal lymphopoietin expression is increased in the horny layer of patients with atopic dermatitis. Clin Exp Immunol. 2013;171(3):330-337
27. Ilves T, Harvima IT. OX40 ligand and OX40 are increased in atopic dermatitis lesions but do not correlate with clinical severity. J Eur Acad Dermatol Venereol. 2013;27(2):e197-e205.
28. Laberge S, Ghaffar O, Boguniewicz M, Center DM, Leung DY, Hamid Q. Association of increased CD4+ T-cell infiltration with increased IL-16 gene expression in atopic dermatitis. J Allergy Clin Immunol. 1998;102(4 Pt 1):645-650
29. Szegedi K, Kremer AE, Kezic S, et al. Increased frequencies of IL-31-producing T cells are found in chronic atopic dermatitis skin. Exp Dermatol. 2012;21(6):431-436
30. Hanifin JM, Thurston M, Omoto M, Cherill R, Tofte SJ, Graeber M. The eczema area and severity index (EASI): assessment of reliability in atopic dermatitis. EASI Evaluator Group. Exp Dermatol. 2001;10(1):11-18
31. Leung DY. Atopic dermatitis: new insights and opportunities for therapeutic intervention. J Allergy Clin Immunol. 2000;105(5):860-876
32. Park HY, Kim CR, Huh IS, et al. Staphylococcus aureus Colonization in Acute and Chronic Skin Lesions of Patients with Atopic Dermatitis. Ann Dermatol. 2013;25(4):410-416
33. Grossmann M, Jamieson MJ, Kirch W. Histamine response and local cooling in the human skin: involvement of H1- and H2-receptors. Br J Clin Pharmacol. 1999;48(2):216-222
34. Amin K. The role of mast cells in allergic inflammation. Respir Med. 2012;106(1):9-14
35. Yamaguchi M, Sayama K, Yano K, et al. IgE enhances Fc epsilon receptor I expression and IgE-dependent release of histamine and lipid mediators from human umbilical cord blood-derived mast cells: synergistic effect of IL-4 and IgE on human mast cell Fc

epsilon receptor I expression and mediator release. J Immunol. 1999;162(9):5455-5465
36. Bohl T. Lichenification Superimposed on an Underlying Preceding Pruritic Disease. Vulvar Disease. 2019:153-155.
37. Boniface K, Bernard FX, Garcia M, Gurney AL, Lecron JC, Morel F. IL-22 inhibits epidermal differentiation and induces proinflammatory gene expression and migration of human keratinocytes. J Immunol. 2005;174(6):3695-3702
38. Seltmann J, Roesner LM, von Hesler FW, Wittmann M, Werfel T. IL-33 impacts on the skin barrier by downregulating the expression of filaggrin. J Allergy Clin Immunol. 2015;135(6):1659-61.e4
39. Howell MD, Kim BE, Gao P, et al. Cytokine modulation of atopic dermatitis filaggrin skin expression. J Allergy Clin Immunol. 2009;124(3 Suppl 2):R7-R12
40. Gutowska-Owsiak D, Schaupp AL, Salimi M, et al. IL-17 downregulates filaggrin and affects keratinocyte expression of genes associated with cellular adhesion. Exp Dermatol. 2012;21(2):104-110
41. Cornelissen C, Marquardt Y, Czaja K, et al. IL-31 regulates differentiation and filaggrin expression in human organotypic skin models. J Allergy Clin Immunol. 2012;129(2):426-433.e4338
42. Sonkoly E, Muller A, Lauerma AI, et al. IL-31: a new link between T cells and pruritus in atopic skin inflammation. J Allergy Clin Immunol. 2006;117(2):411-417
43. Mempel M, Voelcker V, Köllisch G, et al. Toll-like receptor expression in human keratinocytes: nuclear factor kappaB controlled gene activation by Staphylococcus aureus is toll-like receptor 2 but not toll-like receptor 4 or platelet activating factor receptor dependent. J Invest Dermatol. 2003;121(6):1389-1396
44. Yamasaki K, Kanada K, Macleod DT, et al. TLR2 expression is increased in rosacea and stimulates enhanced serine protease production by keratinocytes. J Invest Dermatol. 2011;131(3):688-697
45. Voegeli R, Rawlings AV, Breternitz M, Doppler S, Schreier T, Fluhr JW. Increased stratum corneum serine protease activity in acute eczematous atopic skin. Br J Dermatol. 2009;161(1):70-77
46. Schröder JM. Antimicrobial peptides in healthy skin and atopic dermatitis. Allergol Int. 2011;60(1):17-24
47. Simanski M, Rademacher F, Schröder L, Schumacher HM, Gläser R, Harder J. IL-17A and IFN-γ synergistically induce RNase 7 expression via STAT3 in primary keratinocytes. PLoS One. 2013;8(3):e59531
48. Wolk K, Kunz S, Witte E, Friedrich M, Asadullah K, Sabat R. IL-22 increases the innate immunity of tissues. Immunity. 2004;21(2):241-254
49. Howell MD, Boguniewicz M, Pastore S, et al. Mechanism of HBD-3 deficiency in atopic dermatitis. Clin Immunol. 2006;121(3):332-338
50. Menzies BE, Kenoyer A. Staphylococcus aureus infection of epidermal keratinocytes promotes expression of innate antimicrobial peptides. Infect Immun. 2005;73(8):5241-5244
51. Volpe E, Servant N, Zollinger R, et al. A critical function for transforming growth factor-beta, interleukin 23 and proinflammatory cytokines in driving and modulating human T(H)-17 responses. Nat Immunol. 2008;9(6):650-657
52. Touzot M, Cacoub P, Bodaghi B, Soumelis V, Saadoun D. IFN-α induces IL-10 production and tilt the balance between Th1 and Th17 in Behçet disease. Autoimmun Rev. 2015;14(5):370-375
53. Maier E, Werner D, Duschl A, Bohle B, Horejs-Hoeck J. Human Th2 but not Th9 cells

release IL-31 in a STAT6/NF-κB-dependent way. J Immunol. 2014;193(2):645-654
54. Trifari S, Kaplan CD, Tran EH, Crellin NK, Spits H. Identification of a human helper T cell population that has abundant production of interleukin 22 and is distinct from T(H)-17, T(H)1 and T(H)2 cells. Nat Immunol. 2009;10(8):864-871
55. Vu AT, Baba T, Chen X, et al. Staphylococcus aureus membrane and diacylated lipopeptide induce thymic stromal lymphopoietin in keratinocytes through the Toll-like receptor 2-Toll-like receptor 6 pathway. J Allergy Clin Immunol. 2010;126(5):985-993.e9933
56. Ito T, Wang YH, Duramad O, et al. TSLP-activated dendritic cells induce an inflammatory T helper type 2 cell response through OX40 ligand. J Exp Med. 2005;202(9):1213-1223
57. Martin H, Laborel-Préneron E, Fraysse F, et al. Aquaphilus dolomiae extract counteracts the effects of cutaneous S. aureus secretome isolated from atopic children on CD4+ T cell activation. Pharm Biol. 2016;54(11):2782-2785
58. van Dalen R, De La Cruz Diaz JS, Rumpret M, et al. Langerhans Cells Sense Staphylococcus aureus Wall Teichoic Acid through Langerin To Induce Inflammatory Responses. mBio. 2019;10(3):e00330-19
59. Akdis M, Palomares O, van de Veen W, van Splunter M, Akdis CA. TH17 and TH22 cells: a confusion of antimicrobial response with tissue inflammation versus protection. J Allergy Clin Immunol. 2012;129(6):1438-quiz1451.
60. Kulik L, Maywald M, Kloubert V, Wessels I, Rink L. Zinc deficiency drives Th17 polarization and promotes loss of Treg cell function. J Nutr Biochem. 2019;63:11-18
61. Del Prete G, De Carli M, Almerigogna F, Giudizi MG, Biagiotti R, Romagnani S. Human IL-10 is produced by both type 1 helper (Th1) and type 2 helper (Th2) T cell clones and inhibits their antigen-specific proliferation and cytokine production. J Immunol. 1993;150(2):353-360
62. Webb GJ, Hirschfield GM, Lane PJ. OX40, OX40L and Autoimmunity: a Comprehensive Review. Clin Rev Allergy Immunol. 2016;50(3):312-332
63. Vazquez ML, Kaila N, Strohbach JW, et al. Identification of N-{cis-3-[Methyl(7H-pyrrolo[2,3-d]pyrimidin-4-yl)amino]cyclobutyl}propane-1-sulfonamide (PF-04965842): A Selective JAK1 Clinical Candidate for the Treatment of Autoimmune Diseases. J Med Chem. 2018;61(3):1130-1152
64. Shah DK, Betts AM. Antibody biodistribution coefficients: inferring tissue concentrations of monoclonal antibodies based on the plasma concentrations in several preclinical species and human. MAbs. 2013;5(2):297-305
65. Popovic B, Breed J, Rees DG, et al. Structural Characterisation Reveals Mechanism of IL-13-Neutralising Monoclonal Antibody Tralokinumab as Inhibition of Binding to IL-13Rα1 and IL-13Rα2. J Mol Biol. 2017;429(2):208-219
66. Li Z, Krippendorff BF, Sharma S, Walz AC, Lavé T, Shah DK. Influence of molecular size on tissue distribution of antibody fragments. MAbs. 2016;8(1):113-119
67. Satake I, Tari K, Nakagomi K, Ozawa K. Feasibility and pharmacokinetics of continuous subcutaneous infusion of low-dose interferon-gamma: a pilot study. Jpn J Clin Oncol. 1993;23(6):356-362
68. Carvalho B, Aleshi P, Horstman DJ, Angst MS. Effect of a preemptive femoral nerve block on cytokine release and hyperalgesia in experimentally inflamed skin of human volunteers. Reg Anesth Pain Med. 2010;35(6):514-519
69. D'Ippolito D, Pisano M. Dupilumab (Dupixent): An Interleukin-4 Receptor Antagonist for Atopic Dermatitis. P T. 2018;43(9):532-535
70. Le Floc'h A, Allinne J, Nagashima K, et al. Dual blockade of IL-4 and IL-13 with

dupilumab, an IL-4Rα antibody, is required to broadly inhibit type 2 inflammation. Allergy. 2020;75(5):1188-1204

71. Saito T, Iida S, Terao K, Kumagai Y. Dosage Optimization of Nemolizumab Using Population Pharmacokinetic and Pharmacokinetic-Pharmacodynamic Modeling and Simulation. J Clin Pharmacol. 2017;57(12):1564-1572
72. Oyama S, Kitamura H, Kuramochi T, et al. Cynomolgus monkey model of interleukin-31-induced scratching depicts blockade of human interleukin-31 receptor A by a humanized monoclonal antibody. Exp Dermatol. 2018;27(1):14-21
73. Ambrose C, Colice G, Salapa K, Parnes J, and Corren, J. Effect of Tezepelumab on Exacerbations in Patients with Severe, Uncontrolled Asthma, According to Baseline Body Mass Index: Results from the Phase 2b PATHWAY Study. J Allergy Clin Immunol. 2020:145, AB25
74. Verstraete K, Peelman F, Braun H, et al. Structure and antagonism of the receptor complex mediated by human TSLP in allergy and asthma. Nat Commun. 2017;8:14937
75. Gudi G, Vinu CA, Sunitha GN, et al. Clinical pharmacokinetics and immunogenicity of GBR 830, a first-in-class humanized monoclonal antibody inhibiting OX40 to treat atopic dermatitis. Int Invest Dermatol Meeting. 2018.
76. Macoin J, Blein S, Monney T, et al. GBR 830: An OX40 antagonist antibody with a favorable toxicity profile in non-human primates. J Invest Dermatol. 2018;138:S186-S186
77. Strand V, McInnes I, Mease P, et al. Matching-adjusted indirect comparison: secukinumab versus infliximab in biologic-naive patients with psoriatic arthritis. J Comp Eff Res. 2019;8(7):497-510
78. Bruin G, Loesche C, Nyirady J, Sander O. Population Pharmacokinetic Modeling of Secukinumab in Patients With Moderate to Severe Psoriasis. J Clin Pharmacol. 2017;57(7):876-885
79. Baverel PG, White N, Vicini P, Karlsson MO, Agoram B. Dose-Exposure-Response Relationship of the Investigational Anti-Interleukin-13 Monoclonal Antibody Tralokinumab in Patients With Severe, Uncontrolled Asthma. Clin Pharmacol Ther. 2018;103(5):826-835
80. Zhu R, Zheng Y, Dirks NL, et al. Model-based clinical pharmacology profiling and exposure-response relationships of the efficacy and biomarker of lebrikizumab in patients with moderate-to-severe asthma. Pulm Pharmacol Ther. 2017;46:88-98
81. Koster MI. Making an epidermis. Ann N Y Acad Sci. 2009;1170:7-10
82. Wallace DL, Zhang Y, Ghattas H, et al. Direct measurement of T cell subset kinetics in vivo in elderly men and women. J Immunol. 2004;173(3):1787-1794
83. Prendiville J, Thatcher N, Lind M, et al. Recombinant human interleukin-4 (rhu IL-4) administered by the intravenous and subcutaneous routes in patients with advanced cancer--a phase I toxicity study and pharmacokinetic analysis. Eur J Cancer. 1993;29A(12):1700-1707
84. Ernstoff MS, Trautman T, Davis CA, et al. A randomized phase I/II study of continuous versus intermittent intravenous interferon gamma in patients with metastatic melanoma. J Clin Oncol. 1987;5(11):1804-1810
85. Kamath AT, Henri S, Battye F, Tough DF, Shortman K. Developmental kinetics and lifespan of dendritic cells in mouse lymphoid organs. Blood. 2002;100(5):1734-1741
86. Werfel T, Layton G, Yeadon M, et al. Efficacy and safety of the histamine H4 receptor antagonist ZPL-3893787 in patients with atopic dermatitis. J Allergy Clin Immunol. 2019;143(5):1830-1837.e4

87. Storn R and Price K. Differential evolution–a simple and efficient heuristic for global optimization over continuous spaces. J Global Optimization. 1997;11(4), 341-359
88. Brunner PM, Pavel AB, Khattri S, et al. Baseline IL-22 expression in patients with atopic dermatitis stratifies tissue responses to fezakinumab. J Allergy Clin Immunol. 2019;143(1):142-154